Proceedings of the 1999 IEEE/ASME
International Conference on Advanced Intelligent Mechatronics
September 19-23, 1999 • Atlanta, USA

Design of Air Bearing System for Fine Motion Application of Multi-DOF Spherical Actuators

Dan E. Ezenekwe
Corning Incorporated
Telecommunications Product Division,
310 N. College Road, Wilmington NC 28405

Kok-Meng Lee
George W. Woodruff School of Mechanical Engineering,
Georgia Institute of Technology,
Atlanta GA 30332-0405

Abstract – Fluid bearings play active roles in precision devices, supporting large loads in machinery thereby extending the lifetime of components by reducing wear and tear. Many potential industrial applications of spherical actuators require fine motion control of the output shaft. A non-contact bearing design for such spherical devices offers an interesting method of achieving precision positioning of the output shaft and yet has the potential to enhance their performance in more advanced applications. This paper presents an analytical investigation on the design, modeling of a practical air bearing system for ball-joint-like actuators. Specifically, it discussed design issues and kinematics, and characterizes the air bearing forces of a variable reluctance (VR) spherical actuator. The air bearing system introduces three linear degrees of freedom (DOF) motion to the rotor dynamics and the paper addresses a method of regulating the translations in order to improve the orientation manipulations. The performance of the design is evaluated through improvements in the torque output and dynamic performance of the orientation motion. It is expected that this research will be a basis for designing and evaluating an improved VR spherical motor with enhanced torque capability by eliminating mechanical friction.

1. INTRODUCTION

Many applications in the industry require the use of unconventional actuators to achieve flexibility and precision. A unique example is a novel electromagnetic variable reluctance (VR) spherical actuator developed at Georgia Tech. [1]. The motor offers attractive features of combining three DOF motion (roll, pitch and yaw) in one joint, isotropic properties, large range of motion, no singularities within the workspace and simplicity in structure. These flexible design features make the motor suitable for a wide range of applications such as water-jet cutting, laser cutting, painting, welding, material handling, coordinate measurement etc., where smooth uniform manipulation of the end-effector is required.

The ball-joint-like VR actuator consists of four main subassemblies: 1) the spherical stator, 2) the spherical rotor, 3) the transfer bearings and 4) the orientation measurement system. The spherical rotor, which has orthogonal iron-core poles, is supported inside the stator by transfer bearings. The electromagnetic stator poles are at the apices of a regular polyhedron forming a shell round the rotor. By sequential current-excitation of the stator poles, the reluctance of the air gaps between the bearings and the rotor surface is varied and the rotor responds by re-aligning its poles. Thus, the output shaft could be moved to desired position in Cartesian space. In this research, we are interested to investigate the use of thin film air bearings to support the rotor. Unlike magnetic bearing that is inherently unstable, the air bearing is essentially a regulator that tends to maintain the rotor at its equilibrium position.

Over the years, research has been directed toward the optimization of the motor torque by controlling the orientation motion. Recently, efforts to reduce the discrepancies between the actual and predicted torque outputs have suggested that friction, accountable by the transfer bearings of the motor, is significant. The "reaction-free" magnetic levitation control strategy proposed by Zhou [2] and aimed at relaxing frictional forces was an advancement but not adequate for reasons of practicality and instability without sophisticated feedback control design, for many applications of the VR motor. As advances in technology continue to demand more accurate and high precision spherical devices, opportunities still exist to utilize the unique attractive features of the VR spherical motor to meet these challenges.

This paper discusses a practical means to effectively overcome static and dynamic friction in spherical actuators and aimed at improving the output torque and broadening the tasks they can undertake. We explore air bearing over fluid bearing, magnetic levitation, and the Meissner effect because it is clean, has a cooling effect on interacting components and does not interfere with the actuator electromagnetic system. Researchers [4] [5] [8] have investigated air bearing designs and characteristics. Others [9] [10] have contributed to improving stability of fixed orifice or inherent restrictor bearings. But these works have concentrated on single bearing, single axis bearing devices. In this paper we are interested in the control of multi-DOF spherical actuators using strategically placed sets of air-bearings.

The rest of the paper is organized as follows: First we present the dynamic characteristics of a simple air bearing system, along with the flow-pressure characteristics of the fluid flow regimes. We then present the design and the kinematics of an air

0-7803-5038-3/99/$10.00 © 1999 IEEE

bearing system for a spherical actuator. Next, the system dynamics of the three degrees-of-freedom (DOF) structure is presented followed by the modeling of the actuating forces. The simulation studies three combinations of the actuating forces and is followed by a conclusion.

2. DYNAMIC CHARACTERIZATICS OF AN AIR BEARING

Figure 1 shows a simple, pocketed, orifice compensated bearing. The air bearing is characterized by three distinct flow regions; namely the restrictor, air pocket, and the annulus. Air enters the bearing from a pressure source, passes through the restrictor, flows through the annulus and then exhausts to the atmosphere.

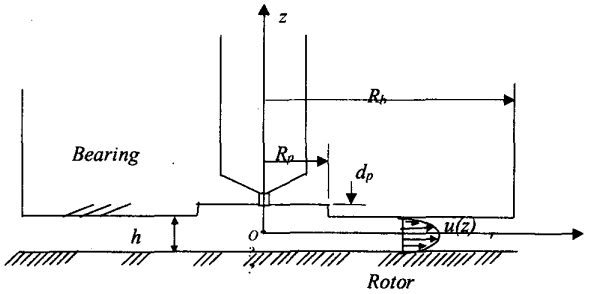

Figure 1 Orifice Compensated Air Bearing

2.1 Governing Equations

Since there is no contact between the surfaces, and frictional effect of air is negligible, the equation of motion for the rotor along the direction of the resultant actuating force is

$$m_r \ddot{h} = 2\pi \left[\int_0^{R_p} p_p r dr - \int_{R_p}^{R_b} p r dr \right] \tag{1}$$

where m_r is the mass of the rotor; p_p and p are the pressure in the pocket and that along the r direction respectively; h, R_p and R_b are the geometrical parameters defined in Figure 1. As shown in Equation (1), the rotor dynamics depend on the pressure-flow relationship in the flow regions.

The time rate of change of the air stored in the gap is the difference between the inflow to the orifice and the outflow through the annulus region, or

$$\frac{dm}{dt} = q_R - q_o \tag{2}$$

where m is the mass of the air stored between the bearing surfaces; and q_R and q_o are the mass flow rates through the orifice restriction and the exhaust through the annulus, respectively.

The flow through an orifice has been modeled by several authors [4]. A particular form known as Fliegner's approximation [5] has been chosen due to its convenience for analytical and computational purposes.

$$q_R = 2\left(\frac{\pi d_o^2}{4}\right)\left[\frac{\gamma}{RT}\left(\frac{2}{\gamma+1}\right)^{\frac{\gamma+1}{\gamma-1}}\left(p_s p_p - p_p^2\right)\right]^{\frac{1}{2}} \tag{3}$$

where q_R, p_s are the flow through the orifice restriction and the pressure at the inlet of the orifice; d_o is the orifice diameter; and R, T, and γ are gas constant, temperature and the ratio of specific heat for air respectively.

Since the air gap is small as compared to the rotor radius, and the rotor surface velocity is much smaller than the fluid velocity, the flow through the annulus is essentially pressure-induced, laminar and is characterized by

$$p^2 = p_a^2 + \frac{12\mu q_o RT}{\pi h^3} ln\left(\frac{R_b}{r}\right) \tag{4}$$

where μ is the absolute viscosity of the air; and p_a denotes the atmospheric pressure.

The air stored between the bearing surfaces can be determined by integrating the product of the volume and the density of air:

$$m = 2\pi \left[\int_0^{R_p} (d_p + h)\rho r dr + \int_{R_p}^{R_b} h\rho r dr \right] \tag{5a}$$

or

$$m = \frac{[hp_p A_{eq} + d_p p_p \pi R_p^2 + hp_a(\pi R_b^2 - A_{eq})]}{RT} \tag{5b}$$

where $A_{eq} = \pi\left[R_b^2 - \frac{2R_b^3 + R_p^3 - 3R_b^2 R_p}{3(R_b - R_p)}\right]$;

ρ is the density of the air; and d_p is defined in Figure 1.

Along with Equations (3), (4) and (5b), Equations (1) and (2) are the non-linear differential equations that describe the pocket pressure p_p and the gap between the two bearing surfaces, h.

2.2 Perturbation Model

For a small gap h, we derive a perturbation model about an operating point by substituting the linear approximations of m, q_R and q_o into Equation (2). Thus, we have

$$a_5\dot{\tilde{p}}_p + a_6\dot{\tilde{h}} = (-a_1\tilde{p}_p + a_2\tilde{p}_s) - (a_3\tilde{p}_p + a_4\tilde{h}) \quad (6)$$

where the notation "~" denotes the small deviations of the quantity of interest;

$$a_1 = \left(\frac{\partial(q_R)}{\partial p_p}\right)\Bigg|_{\substack{p_p=p_{pe}\\ q_R=q_e}} = \frac{q_e}{2p_s}\left(\frac{2-\frac{p_s}{p_{pe}}}{\frac{p_s}{p_{pe}}-1}\right) \quad (6a)$$

$$a_2 = \left(\frac{\partial q_R}{\partial p_s}\right)\Bigg|_{\substack{q_R=q_e\\ p_p=p_{pe}}} = \frac{q_e}{p_s - p_{pe}} \quad (6b)$$

$$a_3 = \frac{\partial(q_o)}{\partial p_p}\Bigg|_{\substack{q_o=q_e\\ p_p=p_{pe}}} = \frac{2q_e p_{pe}}{(p_p^2 - p_a^2)} \quad (6c)$$

$$a_4 = \left(\frac{\partial(q_o)}{\partial h_i}\right)\Bigg|_{h_i=h_e} = \frac{3q_e}{h_e} \quad (6d)$$

$$a_5 = \left(\frac{\partial m}{\partial p_p}\right)\Bigg|_e = \frac{A_{eq}h_e + d_p\pi R_p^2}{RT} \quad (6e)$$

$$a_6 = \left(\frac{\partial m}{\partial h_i}\right)\Bigg|_e = \frac{A_{eq}\left(p_{pe} - p_a\right) + \pi R_b^2 p_a}{RT} \quad (6f)$$

and the subscript "e" denotes the quantity is evaluated at the equilibrium operating point. To obtain the dynamic equation in terms of h explicitly, we assume the linear pressure drop along the annulus and thus Equation (1) becomes

$$m_r\ddot{\tilde{h}} = A_{eq}\tilde{p}_p \quad (7)$$

By substituting the pocket pressure and its time derivative from Equation (7) into Equation (6). The resulting linear equation describing the rotor motion is given as

$$\dddot{\tilde{h}} + \left(\frac{a_1+a_3}{a_5}\right)\ddot{\tilde{h}} + \left(\frac{A_{eq}a_6}{a_5 m_r}\right)\dot{\tilde{h}} + \left(\frac{A_{eq}a_4}{a_5 m_r}\right)\tilde{h} = \left(\frac{A_{eq}a_2}{a_5 m_r}\right)\tilde{p}_s \quad (8)$$

Alternatively,

$$\dddot{\tilde{p}}_p + \left(\frac{a_1+a_3}{a_5}\right)\ddot{\tilde{p}} + \left(\frac{A_{eq}a_6}{a_5 m_r}\right)\dot{\tilde{p}} + \left(\frac{A_{eq}a_4}{a_5 m_r}\right)\tilde{p} = \left(\frac{A_{eq}a_2}{a_5 m_r}\right)\ddot{\tilde{p}}_s \quad (9)$$

As shown in Equation (8) or (9), the air bearing is third order. For a constant supply pressure and with appropriately chosen geometrical parameters, the air bearing could be designed as a regulator so that the rotor tends to return to the equilibrium position regardless of electromagnetic forces or external disturbances.

3. BEARING DESIGN FOR SPHERICAL ACTUATOR

The distribution of bearings on the spherical rotor determines the support forces generated. To maintain the rotor in equilibrium at the stator center, the air bearings are designed to direct their forces at the vertices of polyhedrons towards the stator center. Thus, once the bearing locations are specified, the directions of the bearing forces are considered known.

3.1 Design Configuration

Theoretically, the minimum number of simple point bearings required to achieve bi-directional position control of the spherical rotor in a three-dimensional space is four. To illustrate the minimum force requirement, consider three forces are directed radially toward the origin O of a fixed reference frame. The three points

$$P_1(x,y,z),\ P_2(x,y,z),\ P_3(x,y,z) \in E^3$$

are on a plane defined by

$$\prod(\overrightarrow{P_1P_2}, \overrightarrow{P_1P_3}).$$

Since the points at which the forces act are coplanar, any disturbance in the orthogonal direction to this plane consisting of the line $(\overrightarrow{P_1P_2} \times \overrightarrow{P_1P_3})$ will cause the rotor to lose its equilibrium since the actuating forces are only acting in the direction toward the rotor center. Thus, three point bearings are not adequate to control all three orthogonal translations of the rotor. A forth line of action must be applied against the plane containing the three points. A possible arrangement of minimum number of point bearings on a spherical surface is to locate them at the vertices of a regular tetrahedron on which the sphere is inscribed. A disadvantage of this configuration is that the four point bearings cannot be arranged in pairs for push-pull (regulation) control strategy. The arrangement of a minimum number of bearings is not necessarily attractive since four independent actuators are required.

An alternative arrangement is to alternate the bearings and the stator poles on the limited rotor surface as complements at vertices of polyhedrons. The patterns include tetrahedron-tetrahedron, octahedron-hexahedron, icosahedron-dodecahedron patterns, which correspond to 4/4, 6/8, 12/20 vertices respectively. Figure 2 shows one such example, where the apices of an octahedron in spherical coordinate system are given by

$$\begin{aligned} c_1 &= (1, 0, 0); \\ c_i &= (1, \pi(i-2)/2, \pi/2); \text{ and} \\ c_6 &= (1, 0, \pi). \end{aligned} \quad (10)$$

where i = 2, 3, 4, 5. The vertices of the corresponding complementary hexahedron are at

$c_i = (1, \pi\,(i\text{-}1)/2+\pi/4, \varphi)$ and
$c_j = (1, \pi\,(j\text{-}4)/2\text{-}3\pi/4, \pi\text{-}\varphi)$, (11)
where i = 1, 2, 3, 4 and $j = i+4$; and $\varphi = 54.74^o$ as defined in Figure 2.

Another attractive approach, however, is to design a compound unit so that pressurized air passes through the center of the electromagnetic pole enabling it to also serve as a bearing. The advantages of a compound unit are twofold:

1) The air-jet will provide cooling effect to the electromagnetic pole coil windings.
2) The design will optimize the stator surface by maximizing the size of each bearing, thereby enhancing load-bearing capacity.

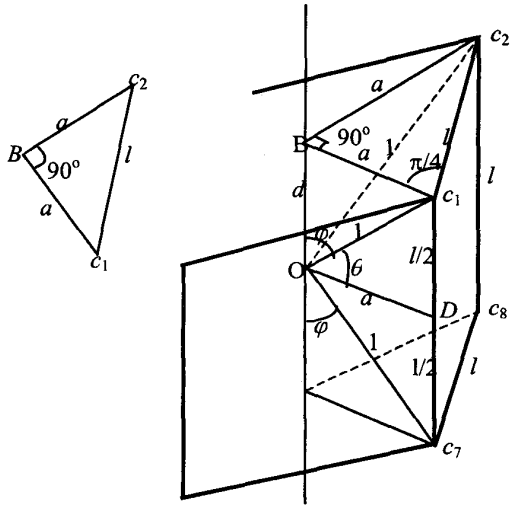

Figure 2: Localized View of a Hexahedron (Cube)

3.2 Kinematics

Consider an arbitrary displacement of the rotor from the center of the stator as shown in Figure 3. For the purpose of design and control, it is of interest to determine both the forward and inverse kinematics. The forward kinematics determines the air gaps, h_i, and h_j between the stator and the rotor along the line of action of a given rotor displacement, $\bar{r}_o$, since the air gap directly governs the magnitude of the actuating forces. The inverse kinematics, on the other hand, defines the rotor position for a given set of air gaps and is essential for the dynamic simulation and analysis. Since direct sensing of the rotor displacement ($\bar{r}_o$) is difficult, the inverse kinematics provides a practical means of computing the rotor position, as the air gaps measurements are more accessible in real-time control.

The kinematic relationship between the air gap and $\bar{r}_o$ is described below. Assuming the homogenous and isotropic rotor, the centers of the rotor and stator are coincident at equilibrium. As shown in Figure 4, the base reference frame XYZ is defined as the center of the stator, O, with the Z-axis pointing toward the opening for the stator. The coordinate system xyz is fixed at the center of the rotor, O', with its z-axis along the rotor output shaft. The gap between the stator and rotor along a pair of forces, $\bar{F}_i$ and $\bar{F}_j$, can be determined with the aid of Figure 5.

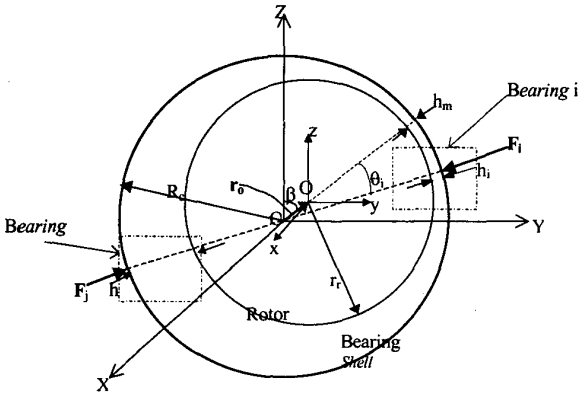

Figure 3. Conceptual Rotor Displacement Geometry

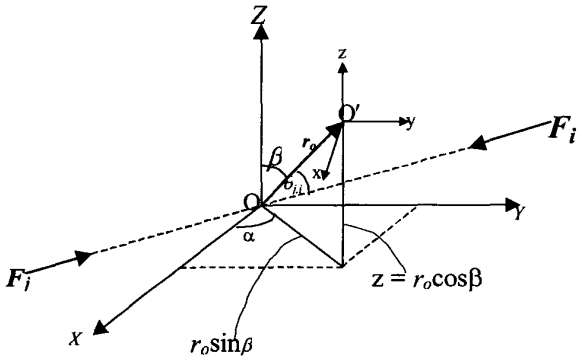

Figure 4. Coordinate System of Spherical Bearing

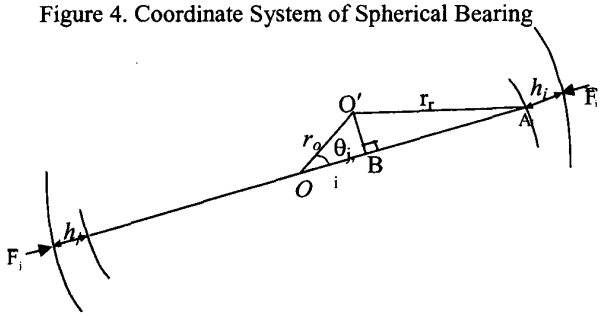

Figure 5 Air Bearing Force Line of Action

The net force, $\bar{F}_{i,j} = \bar{F}_i + \bar{F}_j$, can be described by:

$$\bar{F}_{i,j} = F_{i,j}\bar{e}_{i,j} \tag{12}$$

where $\bar{e}_{i,j}$ is fixed for a given configuration. As shown graphically in Figure 5, the minimum air gap between the rotor is in the direction of $\bar{r}_o$. Thus, the included angle between $\bar{F}_{i,j}$ and $\bar{r}_o$ is

$$\theta_{i,j} = \cos^{-1}(\bar{e}_{i,j}\cdot\bar{e}_{ro}) = \cos^{-1}\left(\frac{\bar{F}_{i,j}\cdot\bar{r}_o}{F_{i,j}\,r_o}\right) \tag{13}$$

The forward kinematics determines the air gaps, h_i, h_j for a given rotor displacement. The gaps govern the magnitude of the actuating forces and are derived from Figure 5 as

$$h_i = r_s - \left\{\sqrt{r_r^2 - r_o^2\sin^2\theta_{i,j}} + r_o\cos\theta_{i,j}\right\} \tag{14a}$$

Since the triangles $\Delta O'BA_i$ and $\Delta O'BA_j$ are similar,

$$h_j = r_s - \left\{\sqrt{r_r^2 - r_o^2\sin^2\theta_{i,j}} - r_o\cos\theta_{i,j}\right\} \tag{14b}$$

It is worth noting that h_j is expressed as a function of $\theta_{i,j}$ and is geometrically related to h_i as shown in Figure 3. Therefore, h_i is computed from h_j in actual implementation or vice versa.

Since direct sensing of the rotor displacement ($\bar{r}_o$) is difficult, the inverse kinematics provides a practical means of computing the rotor position, as the air gaps measurements are more accessible in real-time control. Subtracting Equation (14a) from Equation (14b) yields

$$r_o\cos\theta_{i,j} = \bar{r}_o\cdot\bar{e}_{i,j} = \frac{h_i - h_j}{2} \tag{15a}$$

Two similar equations can be obtained from measuring gaps for two other pairs of forces.

$$\bar{r}_o\cdot\bar{e}_{i-1,\,j-1} = \frac{h_{i-1} - h_{j-1}}{2} \tag{15b}$$

$$\bar{r}_o\cdot\bar{e}_{i+1,\,j+1} = \frac{h_{i+1} - h_{j+1}}{2} \tag{15c}$$

Let $\bar{e}_{i,j}\,(i,j = I, II, III)$ be the directions of 3 gap measurements each of which can be decomposed into the stator fixed X, Y, Z components, then Equations (15a)–(15c) can be written in matrix form:

$$\begin{bmatrix} e_{IX} & e_{IY} & e_{IZ} \\ e_{IIX} & e_{IIY} & e_{IIZ} \\ e_{IIIX} & e_{IIIY} & e_{IIIZ} \end{bmatrix}\begin{bmatrix} X \\ Y \\ Z \end{bmatrix} = \begin{bmatrix} \dfrac{h_i - h_j}{2} \\ \dfrac{h_{i-1} - h_{j-1}}{2} \\ \dfrac{h_{i+1} - h_{j+1}}{2} \end{bmatrix} \tag{16}$$

4. THREE DEGREES-OF-FREEDOM (DOF) DYNAMIC MODELS

The 3-D rotor dynamics is of the form

$$[m_r]\ddot{\boldsymbol{X}} = \boldsymbol{F_m} + \boldsymbol{F_b} \tag{17}$$

where $\boldsymbol{F_m}$ and $\boldsymbol{F_b}$ are the resultant electromagnetic and air-bearing force vectors respectively. In this air bearing system control, the magnetic force is treated as an external disturbance.

4.1 Energy Conversion

The three DOF dynamics can be derived using the principle of energy conservation:

$$\bar{F}_b(t)\cdot\bar{v}(t) = \dot{E}_f \tag{18}$$

where $\dot{E}_f = \sum_{i=1}^{n}\left[p_{si}q_{Ri} - p_{ai}q_{oi} - \frac{d}{dt}\left(\frac{1}{2}C_i p_{pi}^2\right)\right]$; the air capacitance is defined as $C_i = \frac{dm_i}{dp_{pi}}$; n is the number of air bearing units. the fluid power could be rewritten as

$$\dot{E}_f = \sum_{i=1}^{n}\left[(p_{si} - p_{pi})q_{Ri} + (p_{pi} - p_{ai})q_{oi} - \frac{1}{2}p_{pi}^2\dot{C}_i\right] \tag{19}$$

The mechanical power could be written as

$$\bar{F}_b(t)\cdot\bar{v}(t) = \sum_{k=1}^{3}F_{bk}\dot{X}_k \tag{20}$$

where $\dot{X}_k\,(i=1,2,3)$ are the linear velocity components of the rotor or

$$dE_f = (\bar{F}_b\cdot\bar{v})dt = F_{bx}dx + F_{by}dy + F_{bz}dz \tag{21}$$

Noting that the elements, dx, dy and dz, are independent of each other, the gradient of the total energy of the system gives the forces along the tangent lines, we have

$$\bar{F}_b = \nabla E_f \tag{22}$$

where $\nabla \equiv \left(\frac{\partial}{\partial X_1}\right)\bar{E}_1 + \left(\frac{\partial}{\partial X_2}\right)\bar{E}_2 + \left(\frac{\partial}{\partial X_3}\right)\bar{E}_3$ is the gradient of the system's energy along the stator fixed coordinate axes.

In Equation (19), the first and second terms account for fluid frictional dissipation in the orifice and in the annulus respectively. The third term accounts for the fluid energy stored within the air gap, which depends on the volume change (capacitor) and the pressure in the air gap. To serve as an efficient air-bearing, the third term must dominate, otherwise, the fluid energy will be dissipated as frictional heat.

4.2 Ideal Energy Transformation

If the fluid frictional dissipation in the orifice and in the annulus are negligible, the system approaches the case of ideal energy transformation or

$$\vec{F}_b = \nabla E_f = -\frac{1}{2}\sum_{i=1}^{n} p_{pi}^2 \nabla C_i \qquad (21)$$

From the definition of air capacitor and Equation (5b),

$$C_i = \frac{[h_i A_{eq} + d_p \pi R_p^2]}{RT} \qquad (22)$$

and thus,

$$\vec{F}_b = -\frac{A_{eq}}{2RT}\sum_{i=1}^{n} p_{pi}^2 \nabla h_i \qquad (23)$$

Equation (23) shows that the air bearing force is quadratic in p_{pi}. In addition, the force increases as the air gap decreases and thus, the gap tends to stabilize about a steady state operating point.

5. SIMULATIONS

Table 1 lists the parameters determined for the spherical motor [7] where the stator poles and air bearings are both located following the pattern of an Icosahedron. Table 2 tabulates the location of the air bearing on a unit sphere.

Table 1 Parameters used in simulation

Parameters	
Mass m_r,	0.2kg
Outer radius R_b	12.7mm mm
R_b/R_p	16
Supply pressure, p_s	420 kN/m^2
Pressure ratio, p_{pe}/p_s	0.92
Pocket depth, d_p	19.3μm
Orific diameter	0.225mm
Nominal h	69μm

Table 2: Icosahedron Vertices

Bearing	X	Y	Z
c_1	0.89442	0	0.44721
c_2	0.27639	0.85065	0.44721
c_3	-0.72361	0.52573	0.44721
c_4	-0.72361	-0.52573	0.44721
c_5	0.27639	-0.85065	0.44721
c_6	-0.89443	0	-0.44721
c_7	-0.27639	-0.85065	-0.44721
c_8	0.72360	-0.52573	-0.44721
c_9	0.72360	0.52573	-0.44721
c_{10}	-0.27639	0.85065	-0.44721

The air bearing system is simulated using MATLAB for the three degrees-of-freedom rotor translations. The configuration uses five pairs of bearings located on ten of the stator poles without the top and bottom vertices of the Icosahedron. In practical applications, the air bearing system is subjected to an orientation and translation dependent magnetic force trajectory during operation. The system must react to null out the effect of the radial component of the force. We simulate the unknown time dependent force by injecting a force function to the air bearing system dynamics. The force function is given in Figure 6.

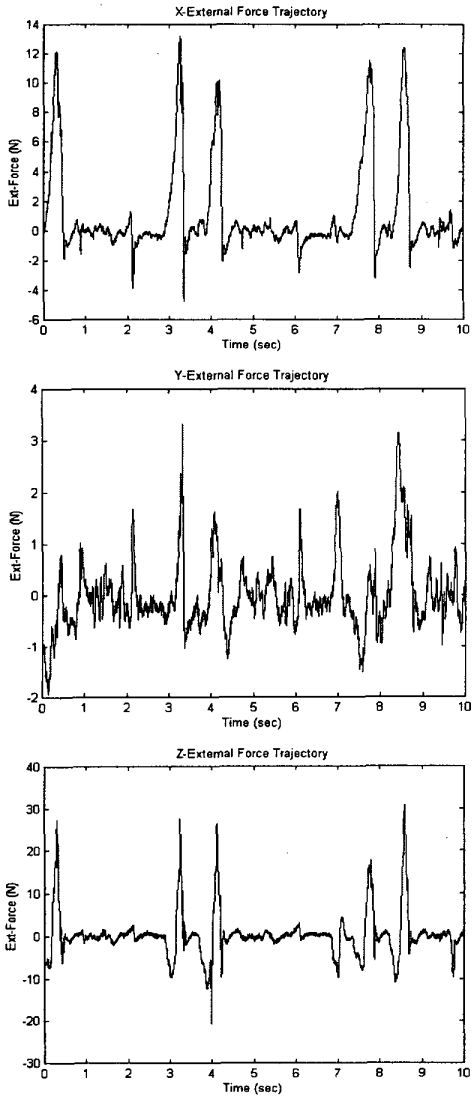

Figure 6 External Force Trajectory

The simulation results are plotted in Figure 7. The results indicate that the magnetic disturbance is adequately compensated by the air-bearing system since the force has little impact on the air bearing dynamics.

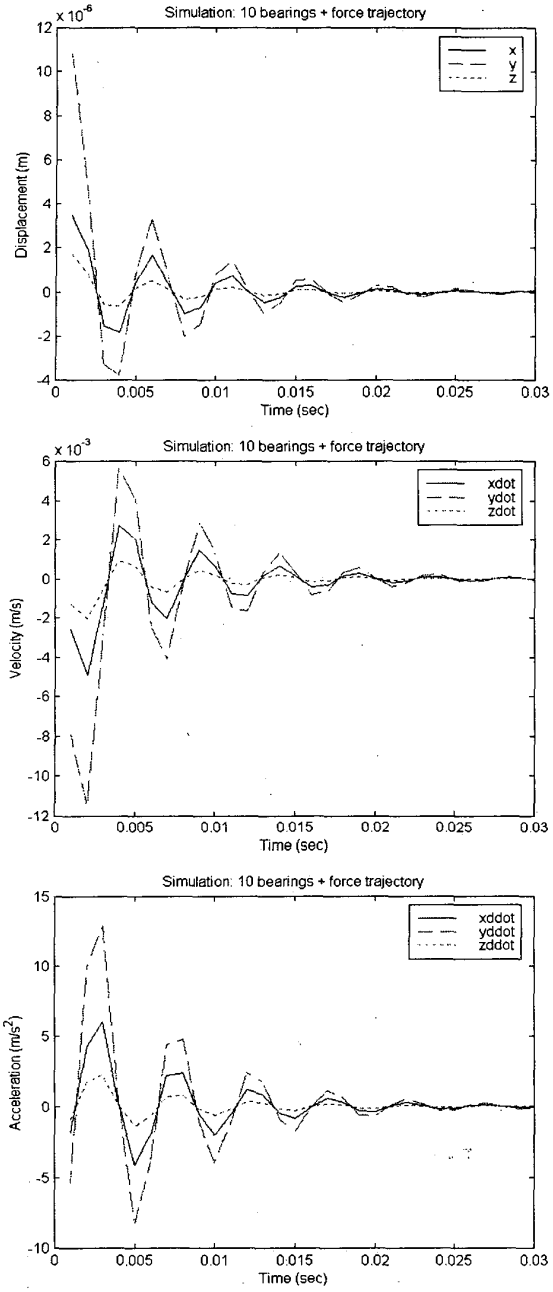

Figure 7: Simulated Rotor Motion

6. CONCLUSIONS

We have presented the modeling, design control of a practical air bearing system for a VR spherical motor. The design uses strategic placement of bearings at the vertices of polyhedrons and external pressurized air to regulate the rotor translations. The forward and inverse kinematics between the rotor displacement and the individual air gaps at positions round the stator are developed in closed-forms, which are essential for design, dynamic simulation and control purposes. Along with the pressure-flow relationship as a function of the rotor position, the paper presents a detailed dynamic model of the air bearing system. The dynamic performance of the air bearing system has been evaluated analytically by simulation.

REFERENCES

[1] Lee, K-M., Vachtsevanos, G., Kwan, C-K., "Development of a Spherical Stepper Wrist Motor", *IEEE International Conference on Robotics & Automation,* 1988.

[2] Zhou, Z., "Real-Time Control and Optimization of a Variable Reluctance Spherical Motor", Ph.D. Thesis, Mechanical Engineering, Georgia Tech., 1995.

[3] Slocum A. H., "Precision Machine Design", Prentice-Hall Englewood Cliffs, NJ, 1992.

[4] Licht, L., Fuller, D. D., Sternlicht, B., "Self-Excited Vibrations of an Air-Lubricated Thrust Bearing", Transactions of ASME, Vol. 80, 1958, pp.411-414.

[5] Licht, L., Elrod, H., "A Study of the Stability of Externally Pressurized Gas Bearings", ASME Journal of Applied Mechanics, Vol. 82, 1960, pp. 250-258.

[6] Ezenekwe, D. E.; "Design Methodology of an Air Bearing System for Multi-DOF Spherical Actuator Motion Control Applications", Ph.D. Thesis, Mechanical Engineering, Georgia Tech., Dec., 1998.

[7] Lee, K.-M., Roth, R., and Zhou, Z., "Dynamic Modeling And Control Of A Ball-Joint-Like Variable Reluctance Spherical Motor," ASME Journal Of Dynamics Systems, Measurements, And Control, Vol. 118, No. 1, March 1996, pp.29-40.

[8] Wilcock, D. F., "MTI Gas Bearing Design Manual", Mechanical Technology Inc., Latham, NY, 1972.

[9]Mori, H., Mori, A. Kaneko, R., Yoshida, K., "Stability Element for External Pressurized Gas Bearing (2nd Report, Stabilizing Element Inserted into the Gas Supply Line)", Transactions of JSME, Vol. 32, No. 244, 1966, pp. 1883-2064.

[10]Ohsumi, T., Ikeuchi, K., Mori, H., Haruyama, H. J., Matsumoto, Y., "Characteristics of a Hydrostatic Bearing with a Controlled Compensating Element", Wear, Vol. 105, April, 1991, pp. 177-194.